This paper appears in IEEE Robotics and Automation Letters (RA-L), 2016.
DOI: 10.1109/LRA.2016.2528301

Mechanics of Tissue Cutting During Needle Insertion in Biological Tissue

Mohsen Khadem[1], Carlos Rossa[1], Ron S. Sloboda[2], Nawaid Usmani[2], Mahdi Tavakoli[1]

***Abstract*—In percutaneous needle insertions, cutting forces at the needle tip deflect the needle and increases targeting error. Thus, modelling needle-tissue interaction in biological tissue is essential for accurate robotics-assisted needle steering. In this paper, dynamics of needle tip interaction with inhomogeneous biological tissue is described and the effects of insertion velocity, tissue mechanical characteristics, and needle geometry on tissue cutting force are studied. Needle interaction with biological tissue is divided into three distinct events and modelled : 1) Initial tissue puncturing, which starts by soft tissue deformation and continues until a crack is formed in the tissue. Employing a viscoelastic model of fracture initiation we have predicted the maximum puncturing force and force-displacement response of a needle in contact with a tissue. 2) Tissue cutting, which follows the crack propagation in tissue and is predicted using a novel energy-based fracture model. The model takes account of the needle tip geometry and the tissue mechanical characteristics. 3) Friction between tissue and needle shaft is estimated during needle insertion and retraction using a needle-tissue friction model. Using a needle driving robot ex-vivo experiments are performed on a porcine tissue sample to identify the model parameters and validate the analytical predictions offered by the models.**

***Index Terms*—Surgical Robotics: Steerable Catheters/Needles, Contact Modelling**

I. INTRODUCTION

ROBOTICS-ASSISTED needle adjustment systems can enhance the efficiency of percutaneous procedures. Modelling the interaction between needle and soft tissue is an essential requirement for robotic needle steering and surgical planning. Here, we investigate the needle-tissue interaction during cutting through biological tissue. The objective of this research is to develop analytical models that accurately predict needle/tissue interaction forces in heterogeneous tissue. Several needle deflection models have been developed that accept these forces as inputs in order to predict needle deflection as an output [1], [2]. We anticipate that the proposed needle/tissue interaction force models will be used more often in needle deflection models, improving realism and performance and enabling future applications in path planning and control of needle deflection in inhomogeneous tissue.

In needle insertion, puncturing the tissue surface and cutting through the tissue results in a relatively large cutting force at the needle tip. A flexible needle with an asymmetric bevelled tip has an uneven distribution of forces at the tip, which causes the needle to bend. For modelling the needle deflection and accurate needle steering, we need a sound understanding of the forces applied to the needle tip during needle insertion.

Modelling the interaction between needle and soft tissue has been the topic of significant research efforts [3]–[5]. In an experimental study, Okamura *et al.* performed ex-vivo tests on bovine liver and measured needle-tissue interaction forces [3] and experimentally obtained the tissue cutting force and assumed it is constant for a given needle and tissue. Misra *et al.* assumed the friction force between the needle shaft and tissue is negligible and incorporated a cohesive zone model to model tissue cutting [4]. Later the cutting force model was implemented in a needle deflection model to predict needle tip location in soft tissue [1]. The authors proposed that the tip forces are primarily governed by the rupture toughness which is assumed to be constant for a given tissue, leading to a constant tissue cutting force. Other researchers empirically studying the effects of cutting force have reported velocity-dependent cutting force at the needle tip [6], [7]. Moore *et al.* used the concept of elementary cutting tool edges, typically used in prediction of cutting forces in machining, to model cutting force in needle insertion [8]. The authors developed a finite element model of tissue cutting which is not computationally efficient for real-time application in robotics-assisted needle steering.

Above mentioned studies treat needle insertion as a quasistatic process neglecting the dynamics of needle insertion, viscoelastic behaviour of tissue, and the effects of insertion velocity on interaction forces. Heverly *et al.* experimentally studied cutting forces and proposed that two distinct phases exist in the evolution of the tissue cutting force [9]: the tissue deflection near the cutting edge and the tissue cutting. Mahvash *et al* extended their approach to study rupture of multilayered biological materials [5]. The authors proposed that the tissue puncturing force can be decreased by increasing insertion velocity; however, during the tissue cutting phase the cutting force remains constant.

In summary, all the mentioned references have neglected

Manuscript received: August, 31, 2015; Revised December, 4, 2015; Accepted January, 24, 2016.

This paper was recommended for publication by Editor Ken Masamune upon evaluation of the Associate Editor and Reviewers' comments. *This work was supported by the Natural Sciences and Engineering Research Council (NSERC) of Canada under grant CHRP 446520, the Canadian Institutes of Health Research (CIHR) under grant CPG 127768 and the Alberta Innovates - Health Solutions (AIHS) under grant CRIO 201201232.

[1] M. Khadem, C. Rossa, PhD, and M. Tavakoli, PhD, are with the Department of Electrical and Computer Engineering, University of Alberta, Edmonton, AB, T6G 2V4, Canada. {`mohsen.khadem, rossa, mahdi.tavakoli`}`@ualberta.ca`

[2] R. S. Sloboda, PhD, FCCPM, and N. Usmani, MD, are with the Cross Cancer Institute and the Department of Oncology, University of Alberta, Edmonton, AB, T6G 1Z2, Canada. {`ron.sloboda, nawaid.usmani`} `@albertahealthservices.ca`

Digital Object Identifier (DOI): see top of this page.

some of the needle-tissue interaction forces or their relation with some of the needle steering variables such as insertion velocity. To the best of the authors' knowledge, all the preceding studies on analytical modelling of tissue cutting proposed a constant velocity-independent cutting force during the tissue cutting phase [3]–[5]. However, other researchers, through empirical studies on the effects of cutting force, have reported velocity-dependent cutting force at the needle tip during tissue cutting [6], [7]. Also, in most researches the effects of friction along the needle shaft on needle-tissue interaction are neglected [1], [4], [8], [9].

We categorize the needle-tissue interaction forces during needle steering in soft tissue into three groups:

1) Tissue puncturing force, F_p: Puncturing happens at the contact point between the needle tip and the tissue surface, starts by deforming the tissue at its surface and continues until the contact force reaches its maximum and a crack is formed in the tissue surface.
2) Tissue cutting force, F_c: Cutting is a dynamic fracture event and starts when the initiated crack propagates into the tissue in response to the needle tip displacement.
3) Friction force, F_f: Friction is applied tangentially to the needle shaft and resists the motion of the needle.
4) Tissue deformation force, F_s: Tissue reaction forces applied perpendicularly to the contact surface between the needle shaft and the tissue.

Fig. 1 displays the above mentioned interaction forces.

We have developed comprehensive mechanics-based models for needle tip interaction with biological tissue. In this paper, we will focus on the forces affecting tissue cutting and puncturing, namely, puncturing, cutting and friction force. Fig. 1(e) shows these forces recorded during needle insertion and retraction in biological tissue. In our previous work we have modelled tissue deformation forces separately [2]. For brevity, tissue deformation forces along the needle shaft are not considered in the analyses that follow.

The main objective of this research is to develop models that accurately predict needle/tissue interaction forces in heterogeneous tissue. We demonstrate the feasibility of predicting interaction forces during needle insertion in biological tissue using fracture mechanics-based models. Our primary contribution is relating the aforementioned interaction forces to needle geometry, the mechanical properties of tissue, and needle insertion velocity. Needle insertion experiments performed on ex-vivo porcine tissue support our proposed modelling approach.

Other contributions of this paper include: (1) Studying tissue puncturing as a two phase event – tissue deformation and crack initiation. Following this approach we can calculate the optimum insertion velocity to cut through tissue without applying excessive force and damaging the tissue or losing control of needle tip as it further slips through the tissue. (2) Studying tissue cutting as a fracture mechanics-based event under two conditions – fixed cutting force under variable tissue displacement and fixed tissue displacement under variable cutting force. By relating the energy release rate under these two conditions to the material resistance we are able to calculate the cutting force as a function of material properties, needle tip geometry, and needle insertion depth. (3) By considering the nonlinear viscoelastic and time-dependent behaviour of soft tissue in all the proposed models, we are able to precisely predict tissue relaxation and creep and consequently their effects on interaction forces and tissue deformation. This allows for prediction of needle-tissue interaction forces during variable-velocity needle insertion and retraction with multiple stops which is the case for clinical needle insertions [10].

This paper is arranged as follows. Section II presents the details of mechanics-based models developed to predict the dynamics of needle-tissue interaction. Ex-vivo experiments performed to identify and validate the proposed dynamical analysis are presented in Section III. Experimental results are evaluated and discussed in Section IV.

II. METHODS

In this section the dynamics of needle interaction with tissue is studied and several mechanics-based models are developed to estimate needle/tissue interaction forces.

A. Tissue Puncturing

Puncturing takes place at the beginning of needle insertion before the needle penetrates the tissue and when the needle tip travels between two different layers of biological tissue. For modelling purposes, we divide the tissue puncturing into two events: (1) Tissue Compression: The needle tip is pressed against the tissue surface and the contact force increases until it reaches its maximum. (2) Crack initiation: When the contact force at the needle tip reaches its maximum value, the tissue in the proximity of the needle tip (failure zone) is severely damaged. The molecular bonds in the failure zone break and a crack is formed in the tissue.

1) Tissue Compression: We will employ a model known as standard linear solid to predict force-deformation response of a needle in contact with a biological tissue during the compression phase. The tissue is modelled as a Newtonian damper and two Hookean springs, one in parallel and one in series. The model has a time-dependent component that enables the modelling of creep, stress relaxation and hysteresis. The model can be expressed as a first order differential equation

$$F + \frac{\eta}{\mu_1}\dot{F} = \mu_2 x + \eta\left(1 + \frac{\mu_2}{\mu_1}\right)\dot{x} \tag{1}$$

where F is the contact force, μ_1 and μ_2 are tissue stiffness, η is the tissue damping coefficient, x is the needle tip displacement, and dot denotes differentiation with respect to time t. Considering the responses of the system in (1) to a unit step force and displacement, and using the convolution integral, the contact force and displacement can be calculated with respect to time as

$$x(t) = \int_0^t C(t-\tau)\frac{dF(\tau)}{d\tau}d\tau \tag{2a}$$

$$F(t) = \int_0^t G(t-\tau)\frac{dx(\tau)}{d\tau}d\tau \tag{2b}$$

where $C(t)$ and $G(t)$ are creep compliance and relaxation modulus, respectively, and are given by

$$C(t) = \frac{1}{E_R}\left[1 - (1 - \frac{\tau_1}{\tau_2})e^{-t/\tau_2}\right] \tag{3a}$$

(a) (b) (c) (d) (e)

Fig. 1. Needle-tissue interaction forces during needle insertion. (a) Tissue puncturing at the contact point between the needle tip and the tissue surface. (b) Tissue cutting including crack propagation into the tissue in response to needle displacement. (c) Needle-tissue friction force applied tangent to the needle shaft. (d) Tissue deformation forces applied perpendicular to the contact surface between the needle shaft and tissue. (e) Force versus displacement curve for needle insertion and retraction in porcine tissue at velocity of 5 mm/sec.

$$G(t) = E_R \left[1 - (1 - \frac{\tau_2}{\tau_1}) e^{-t/\tau_1} \right] \tag{3b}$$

where $E_R = \mu_2$ is the long-time or reference modulus of stiffness, and $\tau_1 = \eta/\mu_1$ and $\tau_2 = (\eta/\mu_2)(1+\mu_2/\mu_1)$ are intrinsic time scales characterizing the nature of the stress relaxation and creep and are called relaxation and retardation times, respectively [11]. Knowing the input force or displacement profile, one can use equation (2a) or (2b) to calculate needle-tissue contact displacement or force during tissue puncturing.

Now, to investigate needle-tissue interaction before the rupture happens, we study the case of needle insertion with a constant velocity V. Using (3b), we have

$$F_p = E_R \left[x_p - V(\tau_2 - \tau_1)(e^{-\dfrac{x_p}{V\tau_1}} - 1) \right] \tag{4}$$

where x_p is the tissue deformation at the contact point. The last term in (4) can be estimated by the first two terms of a Taylor series expansion and (4) reduces to

$$F_p = E_R x_p \frac{\tau_2}{\tau_1} \tag{5}$$

Equation (4) estimates tissue puncturing force as a nonlinear function of velocity. However, (5) states that for relatively high insertion velocities, the puncturing force is almost independent of the needle insertion velocity and increases linearly with respect to the tissue deformation. The velocity at which the puncturing force reaches 90% of its maximum value is called saturation velocity [5]. Using (4) and (5) and 3rd order Taylor expansion, we can calculate the saturation velocity as

$$V_s = 5\frac{x_p}{\tau_1} \tag{6}$$

The above equation can be used to estimate the optimal puncturing velocity for tissue cutting as a function of the tissue viscoelasic parameters and the tissue deformation. The puncturing force increases to its maximum until rupture happens. In the following a fracture mechanics-based analysis is used to calculate the maximum puncturing force.

2) Crack Initiation: In general, failure and crack initiation are characterized by separation of atomic bonds of a material [12]. A local failure criterion typically used to predict crack initiation is the fracture toughness or the crack-resistant force per unit area of crack (G_c) and can include plastic, viscoelastic, or viscoplastic effects depending on the material. A crack initiates and grows when the energy released through crack extension equals or exceeds the fracture toughness. Here, we introduce two parameters typically used to characterize crack initiation and growth in materials, namely, crack-tip-opening displacement (CTOD) and the J contour integral. Next, we use the *Correspondence Principle* [13] to extend the definition of J integral and CTOD to viscoelastic materials and model time-dependent crack initiation in a viscoelastic tissue.

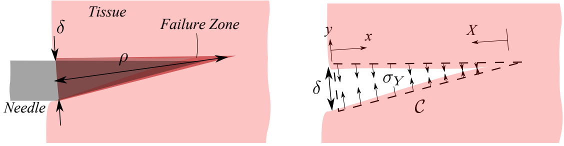

(a) (b)

Fig. 2. A schematic of the Strip-Yield zone model. (a) Plastic failure zone with the length of ρ near the needle tip. δ is the CTOD which is approximately equal to the needle outer diameter. (b) The plastic zone is modelled by a compressive stress σ_Y and $\mathcal{C}$ shown by the dashed line is a contour along the boundary of the Strip-Yield plastic zone.

CTOD and the J integral can be defined and estimated using the Strip-Yield model first introduced by Dugdale [14]. The model is first introduced for small-scale crack in a body loaded by tensile forces such that the crack surfaces move apart in the direction of applied forces.In the Strip-Yield model, yielding is assumed to occur only in a narrow strip zone along the crack line. This strip yield zone or the failure zone is severely damaged and contains voids and discontinuities. In the puncturing phase, when the puncturing force reaches a maximum value, the needle pushes into the failure zone. The failure zone is modelled by the closure yield stress σ_Y acting on the crack faces. Fig. 2 shows a strip yield zone with a length of ρ and the corresponding CTOD, δ.

Now we introduce the J integral as a measure of energy release rate in elastic-plastic materials per unit of crack advance. Considering an arbitrary counterclockwise path ($\mathcal{C}$) around the crack tip (see Fig 2(b)), the J integral is given by

$$J = \int_{\mathcal{C}} \left(w dy - \sigma_{ij} n_j \frac{\partial u_i}{\partial x} ds \right) \tag{7}$$

where w is the strain energy, σ_{ij} are components of the stress tensor, n_j are the components of the unit vector normal to $\mathcal{C}$, ds is a length increment along $\mathcal{C}$ and u_i are displacement vector components.

The J integral and CTOD are used to characterize crack initiation and growth in elastic-plastic fracture. However, these can not be simply used to model time-dependent crack initiation in viscoelastic soft tissue. In order to use the concept of the J integral and CTOD for viscoelastic fracture, we follow the approach proposed by Schapery [13] including the Correspondence Principle. Based on this principle, if the stresses and strains in the elastic body are σ^e_{ij} and ε^e_{ij}, respectively, while the corresponding quantities in the viscoelastic body are

σ_{ij} and ε_{ij}, the stresses and strains are related as follows

$$\sigma_{ij} = \sigma^e_{ij}, \quad \varepsilon_{ij} = E_R C * \varepsilon^e_{ij} \ or \ \varepsilon^e_{ij} = \frac{1}{E_R} G * \varepsilon_{ij} \tag{8}$$

where $*$ is the mathematical shorthand for the convolution operation, E_R is the long-time modulus of stiffness, and C and G are given by (3). Equation (8) allows to find a solution for a viscoelastic problem by an analogy with the solution of the reference elastic problem. We can write the generalized time-dependent J integral using the Correspondence Principle

$$J_v = \int_{\mathcal{C}} \left(w^e dy - \sigma_{ij} n_j \frac{\partial u^e_i}{\partial x} ds \right) \tag{9}$$

where $.^e$ denotes pseudo values related to the elastic reference problem. Now, we compute the J integral for contour $\mathcal{C}$ shown in Fig. 2(b). Considering δ is relatively small ($\simeq 1.5mm$ for needle insertion), the first term in the integral in (9) vanishes because $dy = 0$. Also, the only surface tractions are in the y direction ($n_y = 1$ and $n_x = n_z = 0$), thus

$$J_v = \int_{\mathcal{C}} \sigma_{yy} \frac{\partial u^e_y}{\partial x} ds \tag{10}$$

Let us define a new coordinate XY at the crack tip with $X = \rho - x$. Note that u_y and σ_{yy} only depend on X and $u_y(X = \rho) = \delta/2$. Thus, J_v becomes

$$J_v = 2\int_0^{\rho} \sigma_{yy}(X) \frac{du^e_y(X)}{dX} dX = \int_0^{\delta^e} \sigma_{yy}(\delta^e) d\delta^e \tag{11}$$

Considering σ_{yy} is constant in the failure zone and equal to σ_Y we obtain

$$J_v = \sigma_Y \delta^e \tag{12}$$

Based on the Correspondence Principle, $\delta^e = \frac{1}{E_R} G * \delta$. Note that δ is the CTOD and its maximum value during rupture is equal to the needle outer diameter. Considering constant insertion velocity, we can approximate CTOD as a function of time and needle bevel angle, $\delta = 2Vt\tan(\alpha/2)$, where α is the bevel angle (see Fig. 3(a)). We can calculate δ^e as

$$\delta^e = G * \delta = 2V \tan(\alpha/2) \left[T + (\tau_1 - \tau_2)(e^{-T/\tau_1} - 1) \right] \tag{13}$$

where δ is the CTOD and T is the total time for insertion of the needle tip into the tissue. For constant insertion velocity T is equal to a/V where V is the insertion velocity and a is the length of the needle tip inserted in the tissue at the moment of rupture.

The energy required to advance the needle tip into the tissue is

$$\mathcal{G} = G_c a \delta \tag{14}$$

where G_c is the fracture toughness or the work required to advance the needle tip per unit area of crack. During the rupture event J_v is equal to the material resistance against the needle tip insertion $\mathcal{G}$. Also, the axial forces applied to the tip during rupture can be estimated by $F_p = 2\sigma_Y A_t \sin(\alpha/2)$ where, A_t is the contact area between the needle tip and the tissue. We can estimate the maximum puncturing force during crack initiation (F_p) using (14) and (15)

$$F_p = \frac{A_t G_c a \sin(\alpha/2)}{V \tan(\alpha/2) \left[T + (\tau_1 - \tau_2)(e^{-T/\tau_1} - 1) \right]} \tag{15}$$

Note that at relatively high insertion velocities where $T \ll \tau_1$, the dynamic part of (15) can be estimated by a second order Taylor series expansion. Also, for small bevel angles, $\tan(\alpha/2) = \sin(\alpha/2)$. Thus, (15) reduces to

$$F_p = A_t G_c \frac{\tau_1}{\tau_2} \tag{16}$$

Equation (16) implies that the maximum puncturing force during needle insertion is independent of insertion velocity and is a function of needle-tissue contact area, the ratio of relaxation and retardation time constants, and the rupture toughness of the material.

Using (16), we can quantify the maximum required force to puncture the tissue. Introducing (16) in (5) and (6) we can obtain the optimum insertion velocity for puncturing the tissue

$$V_{opt} = \frac{5 A_t G_c \tau_1}{E_R \tau_2^2} \tag{17}$$

B. Tissue Cutting

Tissue cutting begins after the needle tip is completely inserted into the tissue and the initial crack in the tissue surface is formed. In this section we will use a criterion based on the rate of energy release per unit length of crack advance, to estimate the cutting force applied to the needle tip. As previously discussed, when J is equal to or larger than the material resistance (G_c), crack tip exceeds. It arrests when $J < G_c$. However, many materials do not fail catastrophically at a particular value of J and CTOD and display a rising resistance called the "R curve" [12]. The rise in the R curve is normally associated with the near tip plastic zone or viscoelastic behaviour of the material. The rising R curve typically reaches a steady-state value as the crack length increases. It can be also affected if the growing crack approaches tissue surface or a different layer of tissue.

Materials with rising R curves can be characterized by the fracture toughness at crack initiation, G_c. Using the definition of the R curve, the crack becomes unstable and propagates when

$$\frac{dJ}{da} \geq \frac{dR}{da} \tag{18}$$

where a is the crack length. We will use the criterion given by (18) to predict tissue cutting and estimate the cutting force applied to the needle tip.

To model the needle-tip interaction with soft tissue, the tissue cutting is discreized into small incremental crack growths equal to the size of the needle tip. During tissue cutting, while the needle is being inserted, the tip pushes the tissue back and extends the crack until the CTOD is equal to or bigger than the needle outer diameter so the needle can advance into the tissue. A force distribution with a magnitude of F_c is used to model the needle tip-tissue interaction in the cutting phase (see Fig. 3(a)).

To calculate dJ/da, we use the general definition of the J integral given by

$$J = -\frac{d\Pi}{dA} \tag{19}$$

where $\Pi = \mathcal{U} - \mathcal{W}$, and $\mathcal{U}$ and $\mathcal{W}$ are the strain energy stored in the tissue and the work of the external forces, respectively.

From Fig. 3(a), we have

$$\delta = 2a\tan(\alpha/2) \tag{20}$$

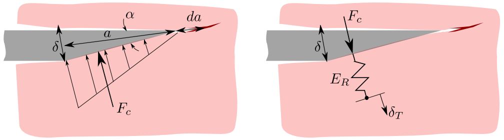

(a) (b)

Fig. 3. Crack propagation in tissue cutting. (a) Needle tip-tissue interface during cutting represented by a force distribution with magnitude of F_c. δ is the crack-tip-opening displacement (CTOD), a is the needle tip length, da is the incremental crack growth. (b) Modelling finite compliance and viscoelastic behaviour of tissue using a linear solid model element. $\delta_t = 0$ is the displacement of the tissue sufficiently far from the crack surface.

Considering that cutting happens at relatively high insertion velocities, we can model the tissue near the needle tip as a linear elastic material. Note that the effects of tissue viscoelastic behaviour are modelled through a time-variant R curve. The cutting force F_c can be calculated using (20) as

$$F_c = \int_0^a E_T \delta da = E_T \tan(\alpha/2) a^2 \tag{21}$$

where E_T is the tissue stiffness per unit length.

First, we consider the case where the cutting force is constant as the crack grows inside the tissue. We can calculate $\mathcal{U}$ and $\mathcal{W}$ as

$$\mathcal{W} = F_c \delta = 2aF_c \tan(\alpha/2) \tag{22a}$$

$$\mathcal{U} = \int_0^\delta F_c \; d\delta = \frac{2}{3} aF_c \tan(\alpha/2) \tag{22b}$$

In (22), we have used (20) to simplify the integrals. Introducing (22) into (19) we have

$$J = -\frac{d\Pi}{dA} = -\frac{1}{w_c}\frac{d\Pi}{da} = \frac{4F_c \tan(\alpha/2)}{3w_c} \tag{23}$$

In (23), we used $dA = w_c da$, where w_c is the crack thickness equal to the needle outer diameter.

To consider the case where the cutting force is not constant and to simulate the finite compliance of the tissue surrounding a growing crack, we follow the approach proposed by Hutchinson and Paris [16]. In this method, a spring is placed at the interface between the needle tip and the tissue, The base of the spring is fixed at a remote distance and the J integral is calculated over a contour including the spring. The proposed modelling approach is schematically presented in Fig. 3(b).

From Fig. 3(b), the displacement of the tissue at a remote distance δ_T is

$$\delta_T = \delta^e + \frac{F_c}{E_R} = 0 \tag{24}$$

where E_R is the tissue long time stiffness modulus. Differentiating δ_T and J and assuming they only depend on load and crack length, we obtain

$$d\delta_T = \left(\frac{\partial \delta}{\partial a}\right)_{F_c} da + \left(\frac{\partial \delta}{\partial F_c}\right)_a dF_c + \frac{dF_c}{E_R} = 0 \tag{25a}$$

$$dJ = \left(\frac{\partial J}{\partial a}\right)_{F_c} da + \left(\frac{\partial J}{\partial F_c}\right)_a dF_c \tag{25b}$$

Fixing δ_T, dividing both sides of (25b) by da, and substituting dF_c/da from (25a), leads to

$$\left(\frac{dJ}{da}\right)_{\delta_T} = \left(\frac{\partial J}{\partial a}\right)_{F_c} - \left(\frac{\partial J}{\partial F_c}\right)_a \left(\frac{\partial \delta}{\partial a}\right)_{F_c} \left[\frac{1}{E_R} + \left(\frac{\partial \delta}{\partial F_c}\right)_a\right]^{-1} \tag{26}$$

Now, we can calculate the components of (26) using (20), (21), and (23)

$$\left(\frac{dJ}{da}\right)_{\delta_T} = \frac{4\tan^2(\alpha/2)}{\dfrac{3w_c}{E_R} + 6w_c\sqrt{\dfrac{\tan(\alpha/2)}{E_T F_c}}} \tag{27}$$

Inserting (27) in (18), we can approximate the cutting force as

$$F_c = \frac{\tan(\alpha/2)}{E_T}\left(\frac{2\tan^2(\alpha/2)}{3w_c dR/da} - \frac{1}{2E_R}\right)^{-2} \tag{28}$$

According to (28) in the case that the tissue around the cutting area is very soft ($E_R \to 0$), the crack propagation arrests and the CTOD increases while the cutting force significantly decreases. However, when the insertion velocity is high and the effects of tissue deformation around the crack can be neglected ($E_R \to \infty$), CTOD is constant and the cutting force is given by

$$F_c = \frac{9w_c^2(dR/da)^2}{4E_T \tan^3(\alpha/2)} \tag{29}$$

From (28) and (29), it can be inferred that at high insertion velocities when E_R is relatively high, the cutting force decreases. Also, the cutting force is a function of $\frac{(dR/da)^2}{E_T}$. As the stiffness of the crack surface (E_T) increases compared to the rate of energy release per unit of crack advancement dR/da, all the work applied to the crack tip leads to crack propagation rather than pushing up the crack surface, and consequently the needle slips through the tissue with a smaller cutting force.

Also, (28) states that the cutting force is not directly dependent on the crack length. However, depending on the R curve of the material it can be affected by velocity and crack length at the beginning of the insertion and when the R curve reaches its steady state, the value of the cutting force becomes almost constant. The rising R-curve can be estimated by the following exponential function

$$R(a) = b_0 \left[1 - exp(-b_1(a - b_2))\right] \tag{30}$$

where b_0, b_1, and b_2 are constant parameters. b_2 denotes the depth at which the crack initiate and a is the crack length equal to the insertion depth. Inserting (30) into (28) gives

$$F_c = \frac{\tan(\alpha/2)}{E_T}\left(\frac{2\tan^2(\alpha/2) exp(b_1(a - b_2))}{3b_3 w_c} - \frac{1}{2E_R}\right)^{-2} \tag{31}$$

where $b_3 = b_0 b_1$. For relatively high insertion depths where $a >> b_2$, (31) simplifies to

$$F_c = \frac{4\tan(\alpha/2)E_R^2}{E_T} \tag{32}$$

Based on (31) and (32) the cutting force initially decreases with insertion depth and eventually converges to a constant value given by (32).

C. Needle-Tissue Friction

In modelling the friction force along the needle shaft, three regimes of interest exist that need to be investigated: (1) Presliding: the friction exists between needle and tissue while the needle is in the stuck state. (2) Break-away: the transition of the needle-tissue between the stuck state and the sliding

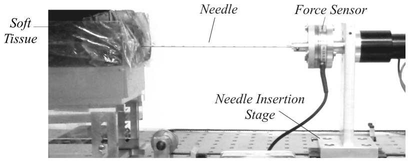

Fig. 4. Experimental setup used to perform needle insertion experiments in porcine tissue. The setup consists of a robotic system with two degrees of freedom (DOF), translational and rotational motions of the needle. Forces and torques are measured at the needle base using a 6 DOF force/torque sensor (JR3, Inc. Woodland, USA).

state. (3) Sliding: contact forces exist in between the needle and soft tissue during the insertion.

The three stages can be accurately explained by LuGre model [17]. The model has been previously used to model needle-tissue friction forces [18]. The model simulates a spring-damper like behaviour at the contact between surface asperities. A complete description of this model can be found in [17]. LuGre model presents the following expression for the friction force:

$$\dot{z} = v - \sigma_0 \frac{|V|}{g(V)} z \tag{33a}$$

$$F_f = \sigma_0 z + \sigma_1 \dot{z} + \sigma_2 V \tag{33b}$$

where F_f is the friction force, z is the elastic deformation of surface asperities, and V is the velocity between the two surfaces in contact. Considering the translational motion of the needle and neglecting tissue displacement, V is equal to the needle insertion velocity. σ_0 is the stiffness coefficient of the microscopic deformations during the pre-sliding displacement, σ_1 is the damping coefficient associated with z, and σ_2 is the viscous damping coefficient. For systems with asymmetry in friction, different values for the parameters can be chosen for positive and negative directions of motion. The $g(v)$ term in (33a) captures the Stribeck's effect and is given by [19]

$$g(v) = f_c + (f_s - f_c)e^{-\Upsilon|v|} \tag{34}$$

where f_s is the stiction friction force, f_c the Coulomb friction, and Υ is a constant coefficient.

III. EXPERIMENTAL VALIDATION

In this section, a series of needle insertion experiments are performed on porcine tissue to 1) identify the tissue puncturing model and statistically validate the dependency of the puncturing force on the velocity as predicted by (4) and the maximum predicted puncturing force estimated by (16), 2) identify the friction force model and validate its dependency on velocity given by (33), and 3) identify and validate the cutting force predicted by (31) and (32).

In order to perform needle insertion into soft tissue, the setup shown in Fig. 4 is used. The needle used to perform insertions is a standard 18-gauge prostate brachytherapy needle (Eckert & Ziegler BEBIG Inc., Oxford, CT, USA) made of stainless steel, with diameter of 1.27 mm and bevel angle of 20°. In all the experiments a shortened needle with the length of 100 mm was used to minimize the effect of tissue deformation and needle bending on recorded forces.

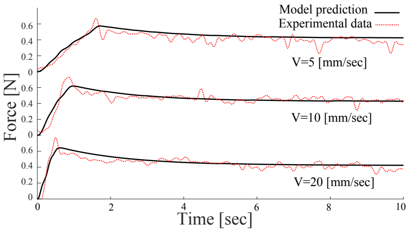

Fig. 5. Results of relaxation tests. Needle force versus time during tissue deformation for velocities of 5, 10, and 20 mm/sec

TABLE I
EXPERIMENTALLY IDENTIFIED MODEL PARAMETERS.

μ_1 [N/mm]	μ_2 [N/mm]	η [N.sec/mm]	τ_1 [sec]	τ_2 [sec]	RMSE [N]
0.0343	0.0557	0.0665	1.9388	5.0872	0.0183

A. *Tissue Puncturing Model*

First, we identify parameters of the tissue puncturing model. Relaxation tests are performed to identify the viscoelastic model given in (1). In the relaxation tests the needle is pressed against the tissue surface and the exerted forces are measured via the force sensor shown in Fig. 4. In the experiments the needle is moved to five different depths (3, 5, 8, 10, and 12 mm) at three different velocities (5, 10, and 20 mm/sec). Three trials were performed for each combination of velocity and depth, leading to a total of 45 relaxation tests. Parameters of the model are identified by fitting the data to (1) using the least-squares method. Tissue model predictions and experimental data for 6 mm tip displacement at three velocities are shown in Fig. 5. Table I provides the values of the identified parameters and Root-Mean-Squared-Error (RMSE) of the fitted model. Root-mean-square error (RMSE) is calculated as $\sqrt{\frac{\sum_{t=1}^{n}(\hat{y}_t - y_t)^2}{n}}$ and is used as a measure of the differences between values predicted by the identified model, $\hat{y}$, and the values actually observed in the experiments, y, for n data points.

The next experiment is designed to validate the model-predicted maximum puncturing force given in (16). The needle is pressed against the tissue until the puncturing happens. We use the identified parameters of the viscoelastic model in (4) to estimate the force-displacement during the puncturing phase and compare it to the recorded data. Ten tissue puncturing experiments were performed. Two sample results are shown in Fig. 6(a). Maximum prediction error and RMSE of the prediction in the ten trials are 0.265 N and 0.107 N, respectively.

Also, fracture toughness (G_c) for the tissue is identified by fitting the model in (16) to the forces measured at the moment of puncturing. Magnitude of estimated rupture toughness per unit area of crack is 132.81 kN/m^3 which is consistent with previous experimentally measured values of rupture toughness for biological tissue samples [4]. In order to measure the magnitude of puncturing force, the needle was inserted in the tissue at 7 different velocities. 5 trials were performed for each velocity. The experimental value of maximum puncturing force for different velocities is shown in Fig. 6(b). As it is predicted by (16) and can be seen in Fig. 6(b) the maximum puncturing force is almost independent of insertion velocity. The estimated maximum puncturing force using (16) is 1.284 N with 95% confidence bounds of ±0.146 N.

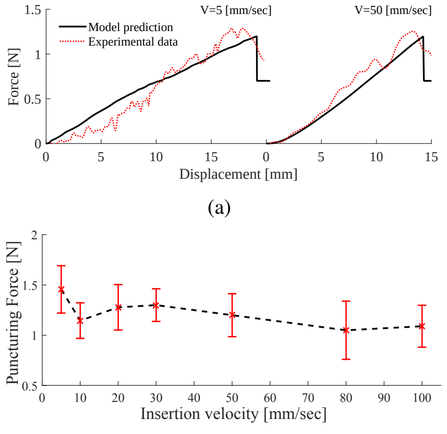

(a)

(b)

Fig. 6. Result of tissue puncturing experiments. (a) Force versus deformation of tissue for velocities of 5 and 50 mm/sec. (b) Average of experimentally-obtained maximum puncturing force versus velocity. Error bars denote standard deviation.

B. Friction Model

In order to identify the parameters of the friction force model, similar experiments as what is presented in [3] is used to separately measure the friction force by eliminating or minimizing the influence of other interaction forces such as the cutting force and the tissue compression force. First, a groove is hollowed out inside the tissue. Next the needle is inserted into the tissue and axial force is measured while the needle tip is in free space in the carved-out track. This force corresponds to needle-tissue friction force plus needle inertia forces. Knowing the acceleration profile and the mass of the needle plus its carrier, we can easily calculate the friction force per unit length of the needle.

To identify the friction model parameters, we employed the procedure based on friction-velocity mapping introduced in [20]. Friction-velocity mapping was developed by performing needle insertions under the aforementioned conditions at different insertion velocities. Five trials were performed. In each trial the needle base displacement was a sinusoidal signal with an initial frequency of 0.05 Hz reaching to 0.2 Hz in 200 seconds, corresponding to insertion velocities of 5 to 40 mm/sec. The RMSE value of the friction force prediction for a single needle insertion and retraction is 0.0016 N/mm. The identified values of the friction model are listed in Table II. Fig. 7 shows the result of friction identification including the estimated friction per unit length of the needle versus time. The magnitude of friction force directly depends on the contact area between the needle shaft and the tissue. In our ex-vivo tests, a porcine tissue with a thin layer of skin and thin layers of connective tissue was used. Thus, we assumed the friction model coefficients are the same for all the layers.

C. Tissue Cutting Model

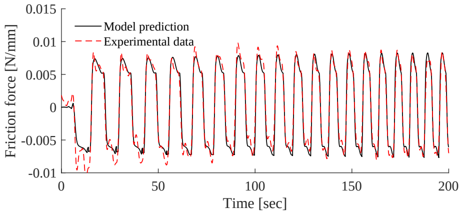

Fig. 7. Experimental and model predicted friction force per unit length of the needle with respect to time.

TABLE II

EXPERIMENTALLY IDENTIFIED PARAMETERS OF THE FRICTION MODEL AND CUTTING FORCE MODEL. NEGATIVE AND POSITIVE DIRECTIONS OF INSERTION ARE DENOTED BY N AND P, RESPECTIVELY.

	σ_0 [N/mm^2]	σ_1 [N.sec/mm^2]	σ_2 [N.sec/mm^2]	f_s [N/mm]	f_c [N/mm]	Υ [sec/mm]
N	0.0521	0.0145	-0.0051	0.294	1.0611	0.0078
P	0.1415	0.0070	0.0049	0.262	0.0974	0.0051
	E_T [N/mm^2]	b_1 [1/mm]	b_2 [mm]	b_3 [N/mm^2]		
	2.4e-3	0.07	5.1	500		

Now that the friction is identified, by subtracting it from recorded axial forces during needle insertion we can measure the cutting force. To identify the cutting force, the needle is manually inserted up to 25 different depths. Next, the axial force at the base of the needle is increased in steps of 0.05 N until the needle begins to move inside the tissue. Knowing the value of crack length at the moment of instability (the depth at which the needle suddenly moves in response to the applied force) and using (31) and (32), we can identify the parameters of the R-curve and estimate tissue stiffness at the crack surface (E_T). Identified values of the cutting force model are given in Table II. The value of model predicted cutting force is presented in Fig.8.

IV. DISCUSSION

In the proposed research, the tissue puncturing is studied as a two phase event – tissue deformation and crack initiation. Equations (5) and (6) can be used to predict contact force between the needle tip and the tissue and its relation to tissue deformation and velocity in the deformation phase. Comparing force response of the needle-tissue system at constant velocities of 5 and 10 mm/sec in Fig. 6, we can see that in the deformation phase, the contact force increases with increasing velocity. This is consistent with (4). Also, according to (5), at high insertion velocities the force response of the system is almost independent of velocity and the force increases linearly with the needle tip displacement. This can be seen by comparing the force responses for velocities of 10 and 20 mm/sec in Fig. 5, where the ratio of force to the needle tip displacement is almost the same. 1.081 and 0.985 for velocities of 10 mm/sec and 20 mm/sec, respectively.

In order to evaluate our proposed analytical models, we compare the experimentally obtained axial forces applied to the needle during a full needle insertion and retraction to the predictions of the identified models. Note that the main three interaction forces studied in this work (i.e., puncturing, cutting, and friction force) can simply be added together to model the

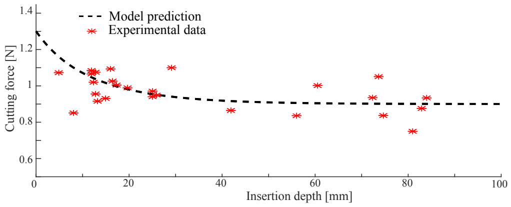

Fig. 8. Experimental and model predicted cutting force vs insertion depth.

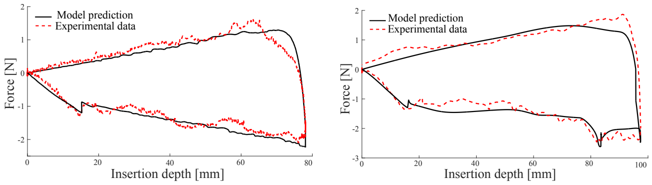

(a) V=5 mm/sec (b) V=100 mm/sec

Fig. 9. Model prediction and experimental data for axial force during needle insertion and retraction at velocities of (a) 5 mm/sec and (b) 100 mm/sec.

overall forces applied to the needle shaft. At the puncturing phase the needle is still outside the tissue and the cutting force and friction are zero. When the needle tip is inserted into the tissue the puncturing force is zero and we have a combination of cutting force and friction (see Fig. 1(e)). Friction is an axial force along the needle shaft and the cutting force is a force applied perpendicular to the needle tip (Fig. 1(c)). Thus the cutting force has two components, an axial and a transverse component. Neglecting the effects of tissue deformation one can say that the axial force recorded at the base of the needle during the needle insertion is the summ of friction and the axial component of the cutting force. During needle retraction the cutting force is zero and there is only friction along the needle shaft.

Combining the force models together as discussed above we can model all the interaction forces during insertion and retraction. Results for insertion velocities of 5 and 100 mm/sec are shown in Fig. 9. Note that in Fig. 9(b) the needle passes through different layers of tissue and there are two puncturing phases at depths of 16.5 (at the beginning of insertion) and 82 mm. RMSE and maximum error of force prediction for velocity of 5 mm/sec are 0.104 N and 0.81 N, respectively. RMSE and maximum error for insertion at 100 mm/sec are 0.182 N and 0.73 N, respectively. It is clear from the figure that the models successfully estimate needle interaction forces with the tissue in all phases of insertion including tissue cutting and puncturing.

As mentioned previously, we have modelled tissue deformation forces separately [2]. For brevity, the effects of tissue deformation on interaction forces are not considered in the presented work. This is the main source of error in the experimental results shown in Fig. 9. Needle deflection and tissue deformation increase as the needle is inserted in tissue. Thus the accuracy of force predictions is reduced as the insertion depth increases.

V. CONCLUDING REMARKS

In this paper, a mechanics based approach is used to model the needle tip interaction with biological tissue during needle insertion. The proposed approach models several events during tissue cutting including: (1) tissue puncturing (2) tissue cutting and propagation of a crack path inside the tissue, and (3) needle-tissue friction along the needle shaft. The model shows a nonlinear relationship between the insertion velocity and tissue puncturing force at low insertion rates. Using a novel viscoelastic fracture based model we were able to predict the maximum puncturing force. Combining the two models we obtained an optimum needle insertion velocity that can be employed to decrease tissue deformation while puncturing the tissue surface. Using a needle driving robot, ex-vivo experiments are performed on a porcine tissue sample to identify the model parameters and validate the analytical predictions. The proposed approach accurately predicts needle insertion forces in inhomogeneous biological tissue. In future work, we intend to relate the predicted tissue cutting forces to the needle deflection. The force models developed in this paper can be implemented in a separate mechanics-based model for needle bending to estimate needle tip trajectory during needle insertion in inhomogeneous biological tissue.

REFERENCES

[1] S. Misra, K. Reed, B. Schafer, K. Ramesh, and A. Okamura, “Mechanics of flexible needles robotically steered through soft tissue,” *Int. J. Rob. Res.*, vol. 29, no. 13, pp. 1640–1660, 2010.

[2] M. Khadem, B. Fallahi, C. Rossa, R. Sloboda, N. Usmani, and M. Tavakoli, “A mechanics-based model for simulation and control of flexible needle insertion in soft tissue,” in *IEEE International Conference on Robotics and Automation (ICRA)*, 2015.

[3] A. M. Okamura, C. Simone, and M. D. O’Leary, “Force Modeling for Needle Insertion into Soft Tissue,” *IEEE Transactions on Biomedical Engineering*, vol. 51, pp. 1707–1716, 2004.

[4] S. Misra, K. Reed, A. Douglas, K. Ramesh, and A. Okamura, “Needle-tissue interaction forces for bevel-tip steerable needles,” in *2nd IEEE RAS & EMBS International Conference on Biomedical Robotics and Biomechatronics(BioRob)*, 2008, pp. 224–231.

[5] M. Mahvash and P. Dupont, “Mechanics of dynamic needle insertion into a biological material,” *IEEE Transactions on Biomedical Engineering*, vol. 57, no. 4, pp. 934–943, 2010.

[6] A. C. Barnett, Y.-S. Lee, and J. Z. Moore, “Fracture mechanics model of needle cutting tissue,” *Journal of Manufacturing Science and Engineering*, 2015.

[7] B. Maurin, L. Barb, P. Bayle, B. Zanne, J. Gangloff, M. de Mathelin, A. Gangi, L. Soler, and A. Forgione, “In vivo study of forces during needle insertions,” in *Proceedings of Medical Robotics Navigation and Visualisation Scientific Workshop (MRNV 04)*, 2004.

[8] J. Z. Moore, K. Malukhin, A. J. Shih, and K. F. Ehmann, “Hollow needle tissue insertion force model,” *(CIRP) Annals - Manufacturing Technology*, vol. 60, no. 1, pp. 157 – 160, 2011.

[9] M. Heverly, P. Dupont, and J. Triedman, “Trajectory optimization for dynamic needle insertion,” in *Proceedings of the IEEE International Conference on Robotics and Automation (ICRA)*, 2005, pp. 1646–1651.

[10] T. Podder, D. Clark, D. Fuller, J. Sherman, and *et.al.*, “Effects of velocity modulation during surgical needle insertion,” in *27th Annual International Conference of the Engineering in Medicine and Biology Society, IEEE-EMBS*, 2005, pp. 5766–5770.

[11] C. Zhang, *Viscoelastic fracture mechanics*. Science Press Beijing, 2006.

[12] T. Anderson, *Fracture Mechanics: Fundamentals and Applications, Third Edition*. Taylor & Francis, 2005.

[13] R. Schapery, “Correspondence principles and a generalized J integral for large deformation and fracture analysis of viscoelastic media,” *International Journal of Fracture*, vol. 25, no. 3, pp. 195–223, 1984.

[14] D. Dugdale, “Yielding of steel sheets containing slits,” *Journal of the Mechanics and Physics of Solids*, vol. 8, no. 2, pp. 100–104, 1960.

[15] T. Azar and V. Hayward, “Estimation of the fracture toughness of soft tissue from needle insertion,” in *Lecture Notes in Computer Science*. Springer Berlin Heidelberg, 2008, vol. 5104, pp. 166–175.

[16] J. W. Hutchinson and P. C. Paris, “Stability analysis of j controlled crack growth,” in *ASTM STP 668, American Society for Testing and Materials*, 1979, pp. 37–64.

[17] C. De Wit, H. Olsson, K. Astrom, and P. Lischinsky, “A new model for control of systems with friction,” *IEEE Transactions on Automatic Control*, vol. 40, no. 3, pp. 419–425, 1995.

[18] A. Asadian, R. Patel, and M. Kermani, “Dynamics of translational friction in needle tissue interaction during needle insertion,” *Annals of Biomedical Engineering*, vol. 42, no. 1, pp. 73–85, 2014.

[19] T. Piatkowski, “Dahl and lugre dynamic friction models the analysis of selected properties,” *Mechanism and Machine Theory*, vol. 73, no. 0, pp. 91 – 100, 2014.

[20] M. Kermani, R. Patel, and M. Moallem, “Friction identification and compensation in robotic manipulators,” *IEEE Transactions on Instrumentation and Measurement*, vol. 56, no. 6, pp. 2346–2353, 2007.